Geometrical Properties of Gel and Fluid Clusters in DMPC/DSPC Bilayers: Monte Carlo Simulation Approach Using a Two-State Model

István P. Sugár,* Ekaterina Michonova-Alexova,* and Parkson Lee-Gau Chong†
*Departments of Biomathematical Sciences and Physiology/Biophysics, The Mount Sinai Medical Center, New York, New York 10029; and †Department of Biochemistry, Temple University, Philadelphia, Pennsylvania 19140 USA

ABSTRACT In this paper the geometrical properties of gel and fluid clusters of equimolar dimyristoylphosphatidylcholine/distearoylphosphatidylcholine (DMPC/DSPC) lipid bilayers are calculated by using an Ising-type model (Sugar, I. P., T. E. Thompson, and R. L. Biltonen. 1999. *Biophys. J.* 76:2099–2110). The model is able to predict the following properties in agreement with the respective experimental data: the excess heat capacity curves, fluorescence recovery after photobleaching (FRAP) threshold temperatures at different mixing ratios, the most frequent center-to-center distance between DSPC clusters, and the fractal dimension of gel clusters. In agreement with the neutron diffraction and fluorescence microscopy data, the simulations show that below the percolation threshold temperature of gel clusters many nanometer-size gel clusters co-exist with one large gel cluster of size comparable with the membrane surface area. With increasing temperature the calculated effective fractal dimension and capacity dimension of gel and fluid clusters decrease and increase, respectively, within the (0, 2) interval. In the region of the gel-to-fluid transition the following geometrical properties are independent from the temperature and the state of the cluster: 1) the cluster perimeter linearly increases with the number of cluster arms at a rate of 8.2 nm/arm; 2) the average number of inner islands in a cluster increases with increasing cluster size, S, according to a power function of $0.00427 \times S^{1.3}$; 3) the following exponential function describes the average size of an inner island versus the size of the host cluster, S: $1 + 1.09(1 - e^{-0.0072 \times S})$. By means of the equations describing the average geometry of the clusters the process of the association of clusters is investigated.

INTRODUCTION

In many biological membranes the proteins and lipid components are organized into domains (Bergelson et al., 1995; Rodgers and Glaser, 1991; Edidin, 1990). Domains are regulating biological functions associated with membranes (Orci et al., 1989; Rothberg et al., 1990). The percolation properties and fractality of the domains affect the equilibrium poise and rates of in-plane reactions and interactions, which may be physiologically important in biological membranes (Thompson et al., 1995; Schram et al., 1996). It was shown that there is a linear relationship between the fractal dimension of the gel domains and the relative diffusion coefficient of the molecules in the fluid phase (Schram et al., 1996). The fractality of the gel domains has a major impact on the mobile fraction of the membrane lipid because highly ramified gel domains are extremely efficient in compartmentalizing the diffusion plane. Micrometer-scale lipid domains have been detected in many cell membranes (Tocanne, 1992; Bergelson et al., 1995) and in dimyristoylphosphatidylcholine/distearoylphosphatidylcholine (DMPC/DSPC) giant unilamellar vesicles (Bagatolli and Gratton, 2000) by fluorescence microscopy. In recent model membrane studies, however, there are indirect (Almeida et al., 1992; Dolainsky et al., 1997; Mendelsohn et al., 1995; Sankaram et al., 1992; Pedersen et al., 1996) and direct (Gliss et al., 1998; Nielsen et al., 2000; Muresan and Lee, 2001) evidences for the existence of much smaller scale—in the nanometer range—lipid domains. Gliss et al. (1998) and Muresan and Lee (2001) imaged gel domains of 10–50 nm by atomic force microscopy (AFM) for the gel-fluid coexistence region in equimolar DMPC/DSPC mixtures. The gel domains exhibited a rather irregular shape. The average center-to-center distance between the small DSPC clusters in an equimolar DMPC/DSPC mixture was estimated to be smaller than 10 nm from neutron diffraction measurements (Gliss et al., 1998).

Biomacromolecules and assemblies of biomolecules are complex systems with complicated structure and dynamics. Theoretical modeling of these systems tries to find the most important interactions sufficient to give a coherent and quantitatively correct description of the observed system properties. Ising-type models, first applied in physics (Ising, 1925) for the theoretical description of magnets, are the most successful coarse-grained models of biomolecules. Typically, the biomolecule or assembly of biomolecules is considered as a system of interacting units arranged on the sites of a lattice. In DNA models of double strand breaking the base pairs are the units situated on the sites of a linear lattice (Sun et al., 1995). In the models of gel-to-fluid transition of lipid membranes different lipid components and/or lipid molecules in gel or fluid states are the units located on the sites of a two-dimensional, usually triangular, lattice (Nagle, 1973; Scott, 1977; Doniach, 1978; Caille et al., 1980; Jørgensen et al., 1993; Sugar et al., 1994, 1999; Jerala et al., 1996). Similar lattice models are used to simulate the interaction of proteins with lipid membranes (Heimburg and Biltonen, 1996; Heimburg and Marsh, 1996;

Received for publication 5 October 2000 and in final form 24 July 2001.
Address reprint requests to Dr. Istvan P. Sugar. Tel.: 212-241-8110; Fax: 212-860-4630; E-mail: sugar@camelot.mssm.edu.

0006-3495/01/11/2425/17 $2.00

Almeida et al., 2001). The folding-unfolding transition of globular proteins is modeled on three-dimensional lattices where the units are the amino acids (Shakhnovich and Gutin, 1993; Yue and Dill, 1995; Hao and Scheraga, 1994, 1996). The partition function of these models cannot be calculated in a closed form. Thus the thermodynamic averages of parameters, characterizing the thermodynamic or structural properties of the system, are calculated by means of Monte Carlo simulations.

The DMPC/DSPC binary mixture is the most thoroughly studied two-component lipid bilayer. The thermodynamic parameters of DMPC/DSPC bilayers have been examined experimentally by a number of methods, including differential scanning calorimetry (Mabrey and Sturtevant, 1976; van Dijck et al., 1977), dilatometry (Wilkinson and Nagle, 1979), neutron scattering (Knoll et al., 1981), nuclear magnetic resonance (NMR) (Lu et al., 1995; Sankaram and Thompson, 1992), electron spin resonance (ESR) (Sankaram et al., 1992), Raman spectroscopy (Mendelsohn and Maisano, 1978), and Fourier transformed infrared spectroscopy (Brumm et al., 1996). The structural characteristics of the fluid and gel coexistence region have been examined experimentally in the mixed systems by fluorescence recovery after photobleaching (FRAP) (Vaz et al., 1989; Schram et al., 1996) fluorescence spectroscopy (Piknova et al., 1996), ESR spectroscopy (Sankaram et al., 1992), neutron diffraction (Gliss et al., 1998), fluorescence microscopy (Bagatolli and Gratton, 2000) and AFM (Gliss et al., 1998; Leidy et al., 2001a; Nielsen et al., 2000; Muresan and Lee, 2001).

These studies have established that DMPC/DSPC forms nonideal mixtures exhibiting positive deviations from ideality. The miscible-type phase diagram has a broad gel-fluid coexistence region bordered by solidus and liquidus lines. The positive deviations from ideality imply that the minor phase forms small clusters in a continuum of the major phase (Von Dreele, 1978). However, the clusters were too small to be detectable directly (Pedersen et al., 1996; Sankaram et al., 1992) and as it was mentioned above, direct detection became possible just recently.

DMPC/DSPC two-component bilayers have been investigated theoretically using the phenomenological theory of regular fluids (Ipsen and Mouritsen, 1988; Brumbaugh et al., 1990; Brumbaugh and Huang, 1992). Von Dreele (1978) used the statistical mechanical description of two-component mixtures to calculate the solidus and liquidus lines of the phase diagram, and like-like as well as like-unlike molecular contacts in the all-gel and all-fluid regions. Priest (1980) and Sugar and Monticelli (1985) have calculated the phase diagrams of a series of two-component phospholipid bilayers using the Landau theory of phase transitions. These models, in which the maximum term or mean-field approximation was utilized, did not provide information about the lateral distribution of the bilayer components, however. Monte Carlo methods have been used to simulate the lateral distribution of the components in the pure gel- or fluid-phase regions of DMPC/DSPC mixtures assuming one state and two components (Jan et al., 1984). Jørgensen et al., (1993) applied a much more complex model to simulate the phase properties and the lateral distribution of components in the one-phase and the gel-fluid coexistence regions of DMPC/DSPC mixtures. The model assumed that each acyl chain could exist in 10 different states, with the interaction between the two lipid species dependent on the incompatibility of acyl chains of different hydrophobic lengths. Risbo et al. (1995) have studied the type of the gel-fluid transition in the same model by using Monte Carlo simulation in the grand canonical ensemble. Risbo and his co-workers pointed out that the gel-fluid transition in the pure DMPC or DSPC system is a continuous transition, but a first-order phase transition can be induced when small amounts of another species are mixed in the pure system. Sugar et al. (1999) described DMPC/DSPC bilayers by a two-state, two-component model in canonical ensemble using a set of parameters derived from a limited amount of experimental data. The analysis of the bilayer energy distribution function revealed that the gel-fluid transition is a continuous transition through equilibrium states for DMPC, DSPC, and DMPC/DSPC mixtures; i.e., the system is above a critical point. By using the same model Sugar et al. (1999) and Sugar and Biltonen (2000) were able to calculate excess heat capacity curves in agreement with the differential scanning calorimetry (DSC) data.

The domain structure of one- and two-component lipid bilayers was also investigated by the above-mentioned theoretical models. The computer simulations of DMPC/DSPC bilayers showed that nanoscale fluid and gel domains exist in the mixed-phase region (Sugar et al., 1999; Nielsen et al., 2000) and pointed out strong positive correlation between the calculated percolation threshold temperatures of gel clusters and the FRAP threshold temperatures detected at different DMPC/DSPC mixing ratios (Sugar et al., 1999).

Molecular dynamics also provide a powerful means to investigate the conformation and dynamics on all-atom models of lipid bilayers involving ~50 lipid molecules in nanosecond time regimes (Huang et al., 1994; Merz, 1997). The following structural properties of single-species lipid bilayers have been successfully emulated by molecular dynamics: hydrocarbon chain order parameters (Huang et al., 1994; Damodoran and Merz, 1994; Tu et al., 1995; Zhou and Schulten, 1995; Perera et al., 1996; Chiu et al., 1995; Feller et al., 1995), amount of water in the solvation shell of phospholipid headgroups (Chiu et al., 1995), fraction of *trans* and *gauche* bonds in hydrocarbon chains (Huang et al., 1994; Chiu et al., 1995), sign and magnitude of dipole potential at the membrane surface (Zhou and Schulten, 1995; Chiu et al., 1995), surface roughness of the membrane and spacial distribution of different molecular groups in the direction normal to the membrane plane (Huang et al., 1994; Damodoran and Merz, 1994; Tu et al., 1995; Zhou and

Schulten, 1995; Perera et al., 1996; Chiu et al., 1995; Feller et al., 1995), and water permeability of the phospholipid bilayer (Marrink and Berendsen, 1994). The technical problems of simulating membranes become more complex when one goes from a single-species lipid bilayer to a system of mixed lipids or of lipids mixed with other types of molecules, such as peptides. This is the case because the relaxation times for different components of a heterogeneous membrane to sample conformations and orientations relative to each other are orders of magnitude longer than the nanosecond time scale sampled by molecular dynamics (Vaz et al., 1989). Similarly, the distance scales over which membrane domains organize themselves are often larger than 10 nm^2, a surface area typical of the largest molecular dynamics simulation to date. A combined application of molecular dynamics and Monte Carlo methods can speed up the equilibration process substantially (Scott et al., 1998); however, to perform simulations on the distance scale of membrane domains, one has to use simple coarse-grained models such as the above-mentioned lattice models.

In this paper a two-state, two-component lattice model of DMPC/DSPC (Sugar et al., 1999) is utilized to simulate the equilibrium lateral distribution of gel- and fluid-state lipid molecules in the mixed phase region. The geometry of the clusters is characterized by size, linear size, perimeter, number of arms, and number and size of inner islands. The statistical analysis reveals the trend in the cluster size dependence of these strongly fluctuating geometrical properties and gives an insight into the process of cluster growth. The calculated averages are compared with relevant experimental data from ESR, neutron diffraction, FRAP, fluorescence microscopy, and AFM.

In physics the above geometric properties of clusters of two-dimensional lattice models have been thoroughly investigated (Klein and Coniglio, 1981; Binder and Stauffer, 1986, 1987; Coniglio, 1989). The physical models, however, are not equivalent with our membrane model because the units are either not pairwisely connected and/or the energy levels of the units are not degenerated, and/or different part of the phase space is investigated. These qualitative differences put our model into a different universality class. For example, in the case of a two-component system, where the components are independent and situated on the sites of a triangular lattice, the percolation threshold concentration is 0.5 (Stauffer, 1985), while in our membrane model, where neighbor units are chemically connected, it is 0.24 (Sugar et al., 1999).

METHODS

Model

A simple Ising-type model is utilized to simulate DMPC/DSPC lipid bilayers. The detailed description and validation of the model have been published elsewhere (Sugar et al., 1999; Sugar and Biltonen, 2000). In this section only an abbreviated description of the model is presented.

A monolayer of the bilayer is modeled as a triangular lattice of N lattice points. Each lattice point is occupied by one acyl chain of either DMPC or DSPC molecules representing component 1 or component 2, respectively. Nearest-neighbor pairs of similar acyl chains are interconnected forming either DMPC or DSPC molecules numbering $N_1/2$ and $N_2/2$, respectively. Every lattice point can exist in two states, corresponding to the gel (g) and fluid state (l). The actual configuration of the monolayer is defined by the component and state at every lattice point and by the connections between the pairs of lattice points.

The intrachain energy, E_i^m, of an acyl chain of component i in state m is assumed constant and independent of location and orientation of the rotational isomers. The number of possible locations and orientations of the rotational isomers is characterized by f_i^m, the degeneracy of the energy level of component i in state m. E_{ij}^{mn} is the interaction energy between component i in state m and component j in state n. Only nearest-neighbor interactions between lattice points are considered because van der Waals interactions between the acyl chains are short-range. By introducing periodic boundary conditions we could eliminate lattice edge effects and substantially reduce the number of model parameters. When fitting the model to a limited number of calorimetric data the strategy of consecutive parameter estimation was utilized to get a robust set of model parameters (see the Determination of Model Parameters section and Table 1 in Sugar et al. (1999)). The analysis of the bilayer energy distribution function revealed that the gel-fluid transition is a continuous transition through equilibrium states for DMPC, DSPC, and DMPC/DSPC mixtures, i.e., the system is above a critical point.

Monte Carlo methods

By using Monte Carlo methods one can simulate the thermal fluctuations of the DMPC/DSPC bilayer. The detailed description of the utilized Monte Carlo methods has been given elsewhere (Sugar et al., 1999). Each simulation starts from an all-gel or all-fluid state, and every molecule is oriented horizontally. Trial configurations of the system are generated by three different elementary steps: 1) by changing the state of a randomly selected acyl chain; 2) by exchanging two randomly selected molecules of different lipid components; and 3) by changing the orientation of two randomly selected nearest-neighbor molecules. A trial configuration is accepted or rejected according to the Metropolis method. This method of decision-making drives the system toward thermodynamic equilibrium, the Boltzmann distribution over the configurations, independently of the choice of the initial configuration.

In a Monte Carlo simulation a chain of elementary steps generating trial configurations is repeated. During this chain of elementary steps, the Monte Carlo cycle, the system has the opportunity of realizing all of its configurations at least one time. In our simulations a Monte Carlo cycle starts with $2N$ trials of local state alterations [during N consecutive trials each lattice point has one opportunity (on average) to change its state and the system to realize any of the 2^N configurations of gel/fluid states], and it is followed by $N_1/2$ (or $N_2/2$ if $N_2 > N_1$) trials of exchange of different molecules, and finally $4N/3$ trials of reorientation of a pair of molecules is performed. The last trial of each Monte Carlo cycle alters the state of every chain. This global, nonphysical state change may accelerate the attainment of the equilibrium distribution (Sun and Sugar, 1997).

In this work an equimolar mixture of DMPC/DSPC bilayers is simulated at different temperatures of the gel-to-fluid transition region. In every simulation the lattice size is 40×40. It was pointed out that in the case of an equimolar mixture of DMPC/DSPC the finite size effects on excess heat capacity are negligibly small at this lattice size (Sugar and Biltonen, 2000). Each simulation starts with 6000 Monte Carlo cycles to attain the equilibrium distribution over the configuration space, and then 120,000 Monte Carlo cycles are performed. After attaining the equilibrium at the end of each cycle the snapshot is analyzed, i.e., the clusters are labeled and counted by using the program of Binder and Stauffer (1987), the geomet-

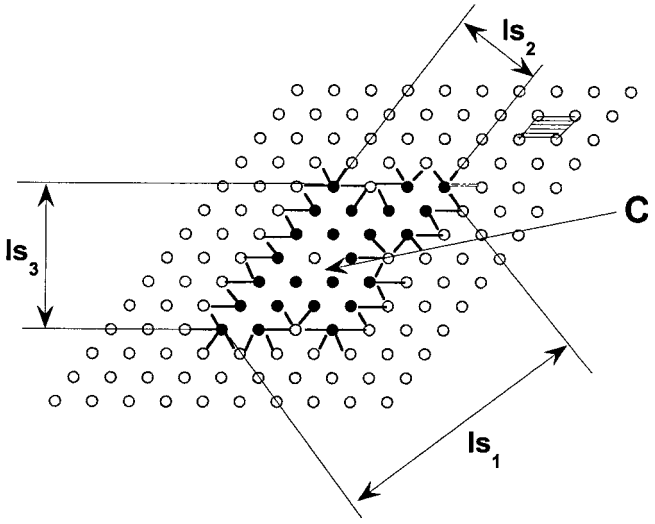

FIGURE 1 A typical gel state cluster with one inner island. *Closed circles*: gel state lattice point; *open circles*: fluid state lattice point. Gel-fluid nearest-neighbor lattice points are interconnected by solid lines at the outer periphery of the cluster. The shaded area in the upper corner marks a unit cell of the lattice. ls_1, ls_2, and ls_3 are the lengths of the projections of the cluster in the three characteristic directions of the lattice. The arrow marks the center of the cluster, *C*, calculated by Eqs. 4 and 5.

rical properties of the clusters are determined, and the data are stored for final statistical evaluation.

Geometry of individual clusters

A typical cluster is shown in Fig. 1. Closed and open circles represent gel and fluid state hydrocarbon chains of the phospholipid molecules, respectively. A gel state cluster may contain *inner islands* of fluid state, or vice versa. In Fig. 1 the host gel state cluster has one inner island ($NI = 1$) of the size of one lattice point ($SI = 1$). The *size* of this gel state cluster ($S = 24$) is defined by the number of hydrocarbon chains belonging to the cluster, or by the surface area of the cluster, *s*:

$$s = S \times (\sqrt{3}/2) \times l^2 \tag{1}$$

where *l* is the unit length of the triangular lattice and $(\sqrt{3}/2) \times l^2$ is the area of a unit cell. The surface area per chain, s/S, depends on the component and the state of the chain. The experimental area/chain in the dipalmitoylphosphatidylcholine (DPPC) bilayer is $s_g/S = 20$ Å^2 for gel and $s_l/S = 32$ Å^2 for the fluid state chain (Wilkinson and Nagle, 1979; Nagle and Tristram-Nagle, 2000). [Experimental specific surface area data are not available for DSPC. We use DPPC data to estimate the unit length in equimolar DMPC/DSPC mixture because every geometric property of this molecule is between the respective properties of DMPC and DSPC.] By using Eq. 1 the interchain distance in gel and fluid clusters is $l_g = 4.8$ Å and $l_l = 6.1$ Å, respectively. One can also define the *linear cluster size*, *ls*, of any cluster by

$$ls = \max\{ls_1, ls_2, ls_3\} \tag{2}$$

where ls_1, ls_2, ls_3 are the lengths of the projections of the cluster in the three characteristic directions of the triangular lattice. In the case of the gel cluster in Fig. 1, $ls_1 = 9 \times (\sqrt{3}/2) \times l$, $ls_2 = 3 \times (\sqrt{3}/2) \times l$, and $ls_3 = 6 \times (\sqrt{3}/2) \times l$, and thus according to Eq. 2 the linear size of the gel cluster is $ls = 9 \times (\sqrt{3}/2) \times l$.

The *periphery* of a cluster is defined by its gel-fluid interface. The interface between the inner islands and the cluster is the *inner periphery* of the cluster, while the rest of the periphery forms the *outer periphery*. In Fig. 1 each gel state chain at the outer periphery of the gel state cluster is connected by lines to its nearest neighbor fluid state chains. The *outer perimeter of the cluster*, *PO*, is defined by the number of these connecting lines ($PO = 48$). This definition of the outer perimeter is found to be very helpful when counting the number of arms of the cluster. Another definition of the outer perimeter is the circumference of the polygon, *po*, which can be drawn around the cluster. [The nodes of the polygon are located at the midpoint of each line interconnecting nearest-neighbor gel and fluid state chains at the cluster's outer periphery.] The circumference of the polygon, *po*, is related to *PO* as follows:

$$po = (PO/2) \times l. \tag{3}$$

where *l* is the unit length of the triangular lattice.

The irregular *shape of the cluster* can be characterized by a vector. Each vector element is equal with the number of lines emanating from one of the lattice points surrounding the cluster. As an example, let us walk clockwise round the gel cluster in Fig. 1, starting from the fluid state lattice point at the upper right corner of the cluster (marked by a double line). The number of lines emanating from each of the 27 fluid state lattice points surrounding the cluster is: 1, 2, 2, 1, 4, 1, 2, 2, 1, 1, 4, 1, 2, 1, 1, 2, 2, 2, 2, 2, 1, 1, 4, 1, 2, 1. Each element of this shape vector locally characterizes the shape of the gel cluster. At the convex, straight, and concave sections of the cluster periphery the vector element is 1, 2, and larger than 2, respectively. The shape vector helps us to determine the *number of arms of the cluster*. We use the following definition of an arm: an arm begins and ends with a concave section, and between these consecutive concave sections there are at least three convex sections. [In the definition at least three convex sections are required, otherwise small bumps and humps would be considered as arms, too.] For example, in the case of the above shape vector the 5th and 11th vector element define the beginning and end of an arm because between these consecutive concave sections there are three 1's defining the convex sections of an arm. Analyzing the complete shape vector we find a total of four arms of the gel cluster in Fig. 1.

The coordinates of the *center of a cluster*, (x_c, y_c), are defined by the following equations:

$$x_c = (1/S)\sum_{i=1}^{S} x_i \tag{4}$$

$$y_c = (1/S)\sum_{i=1}^{S} y_i \tag{5}$$

where x_i and y_i are the coordinates of the *i*th cluster element. In Fig. 1 an arrow points to the center of the gel cluster. By using the above two equations we calculate the center-to-center distance distribution of DSPC compositional clusters in equimolar DMPC/DSPC mixtures.

Thermodynamic averages of cluster geometry

By means of Monte Carlo methods one can simulate the thermal fluctuations of the configurations of DMPC/DSPC bilayers. In our simulations the attainment of equilibrium fluctuations is accelerated by using the nonphysical trial step of global state change at the end of each Monte Carlo cycle (Sun and Sugar, 1997). After attaining the equilibrium the following geometric properties of the clusters are determined from the snapshots at the end of every Monte Carlo cycle: the size, linear size, center, perimeter, number of arms, number of inner islands, and size of inner islands of every gel and fluid cluster. From the data the equilibrium distribution of the cluster size, $P(S)$, the distribution of the center-to-center distance, and the cluster size dependence of the following thermodynamic averages are calculated: average linear size, $\langle ls(S) \rangle$, average outer perimeter, $\langle PO(S) \rangle$,

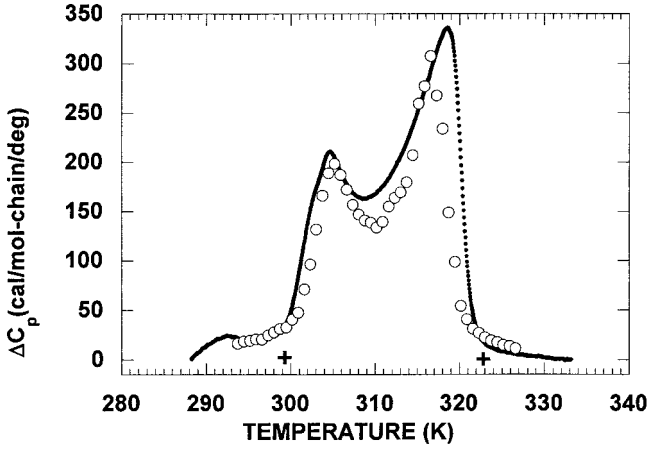

FIGURE 2 Calculated and experimental excess heat capacity curves of equimolar DMPC/DSPC bilayers. *Dotted line*: experimental excess heat capacity curve; *open circles*: calculated values. All calorimetric scans were performed on a home-made high-sensitivity scanning calorimeter (Suurkuusk et al., 1976) at scan rates from 0.1 to 5°C/h. In this scan the lipid concentration was 20 mM with a scan rate of 5°C/h. To obtain the calculated excess heat capacity, C_P, the variance of the lattice energy E was determined at each temperature, T, and then the following equation was used: $C_P \approx C_V = \langle (E - \langle E \rangle)^2 \rangle / (RT^2N)$, where $R = 2$ cal/mol−chain/deg, and N is the number of lattice points. A straight line is fitted to the inflection points of the excess heat capacity curve at its low- and high-temperature edges. The intercepts of the straight lines with the line at zero excess heat capacity define the onset and completion temperatures of the gel-to-fluid transition (see crosses at 299.2 and 322.9 K, respectively).

average number of arms, $\langle NA(S) \rangle$, average number of inner islands, $\langle NI(S) \rangle$, average size of inner islands, $\langle SI(S) \rangle$.

RESULTS AND DISCUSSION

The DMPC/DSPC model described in the Methods section can be used to calculate different thermodynamic averages of the system. Sugar and Biltonen (2000) calculated the excess heat capacity curves of DMPC/DSPC mixture at nine different mole fractions. As an example, Fig. 2 (reproduced from Sugar and Biltonen, 2000), shows the calculated (*open circles*) and experimental (*dotted line*) excess heat capacity curves only for the equimolar DMPC/DSPC mixture. The excellent agreement between the experimental and calculated excess heat capacity curves prompts us to calculate geometrical properties of the clusters by using the same model and compare them with the respective experimental data when they are available.

Cluster size distribution

The size distributions of fluid clusters in an equimolar mixture of DMPC/DSPC are shown at three different temperatures in Fig. 3. Close to the onset temperature of the gel-to-fluid transition, at 302 K the distribution is unimodal and the maximum is located at cluster size $S = 1$. With increasing temperature first a shoulder (Fig. 3 *B*), then at even higher temperature an extra peak appears at larger cluster sizes, i.e., the distribution becomes bimodal (Fig. 3 *C*). This bimodal distribution can be separated into two unimodal ones: the size distribution of the largest cluster of the snapshots (*open circles* in Fig. 3 *D*) and the size distribution of all of the other clusters of the snapshots (*closed circles* in Fig. 3 *D*). The separation shows that the extra peak in Fig. 3 *C* refers to the size distribution of the largest cluster of the snapshots. It is important to note that Fig. 3, *A–D* show only the lower part of the distributions with frequencies $<3 \times 10^{-4}$. With decreasing cluster size the frequency increases continuously up to ~0.6 at cluster size $S = 1$. One should also note that the size distribution of gel clusters changes from unimodal to bimodal with decreasing temperature (not shown). The size distribution of clusters in DMPC/DSPC mixtures was not measured, but the following observations are consistent with a bimodal size distribution. On one hand, neutron diffraction data showed very small DSPC clusters in the nanometer range (Gliss et al., 1998) [in equimolar DMPC/DSPC bilayer the gel clusters are at most twice as large as the DSPC clusters because from the phase diagram it follows that the mole fraction of DSPC in the gel clusters is larger than 0.5], while at similar conditions an at least three orders of magnitude larger gel cluster (or a small number of large gel clusters) was visible in the gel-fluid mixed phase region by fluorescence microscope (Bagatolli and Gratton, 2000).

Cluster size averages

Linear cluster sizes

Depending on the shape of the clusters of size S, their linear size $ls(S)$ can be different. In Fig. 4 *A* the calculated average of the linear size, $\langle ls \rangle$, of gel and fluid clusters are plotted against the cluster size S. The curves in Fig. 4 *A* were calculated from a simulation of equimolar DMPC/DSPC mixture at 305.3 K, but practically the same curves were obtained for simulations at other temperature and mole fraction pairs within the gel/fluid mixed state region. In the rest of the paper one can use these curves to recalculate cluster size to average linear cluster size at a broad range of temperature and mole fraction of DMPC/DSPC mixtures.

Small clusters

At any temperature of the gel-to-fluid transition, if the largest cluster of each snapshot is excluded most of the remaining clusters are very small, and thus the average of their size is small. Fig. 4 *B* shows the average total size and average number of these small clusters in the case of a 40×40 lattice. Both the average total size and the average number of small clusters have a maximum at an intermediate temperature where 10% of the lattice points are occupied

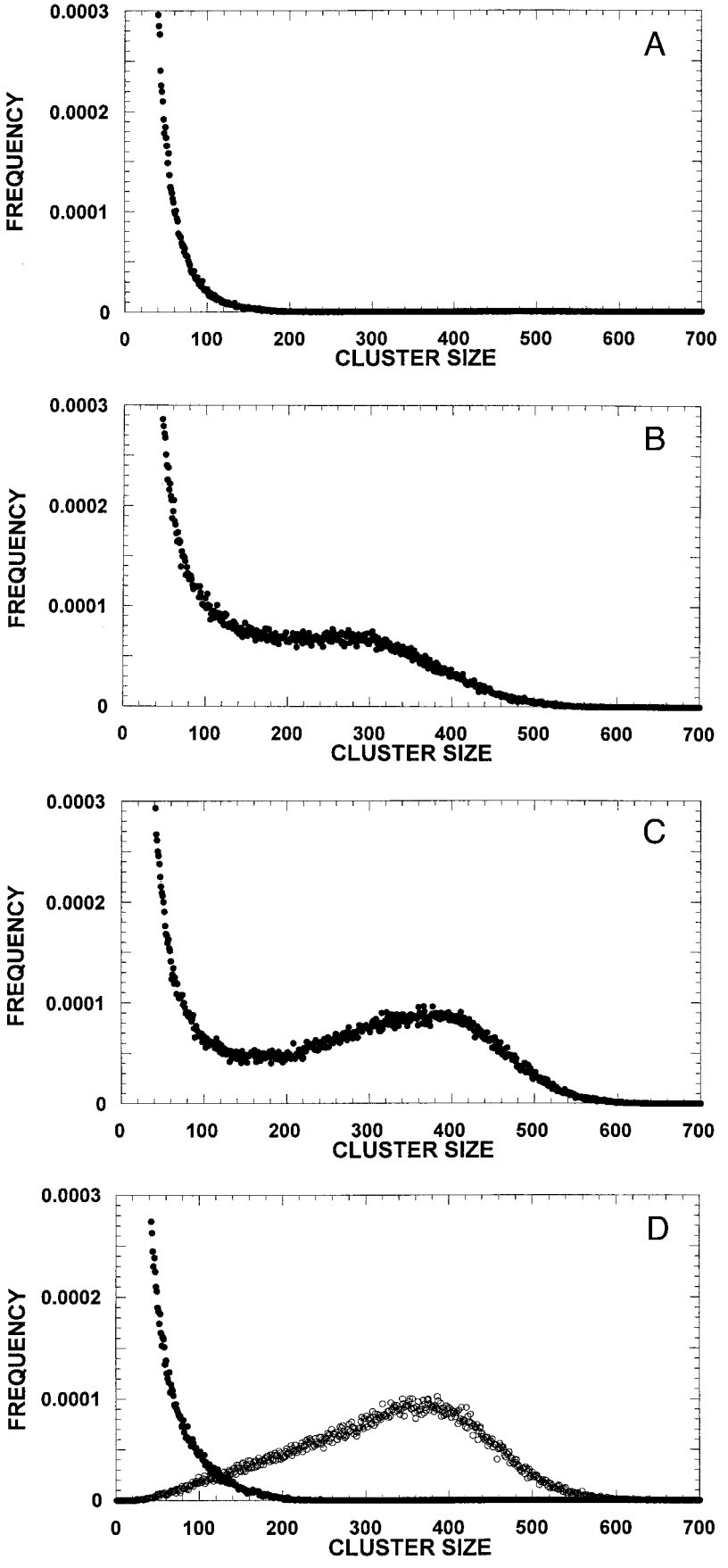

FIGURE 3 Calculated size distributions of fluid state clusters of equimolar DMPC/DSPC bilayers. (*A*) 302 K; (*B*) 305.3 K; (*C*) 306 K; (*D*) 306 K; where open circles mark the size distribution of the largest fluid cluster in each snapshot and closed circles show the size distribution of all the fluid clusters except the largest ones. The average size of these smaller clusters is $\langle s \rangle = 3.19$.

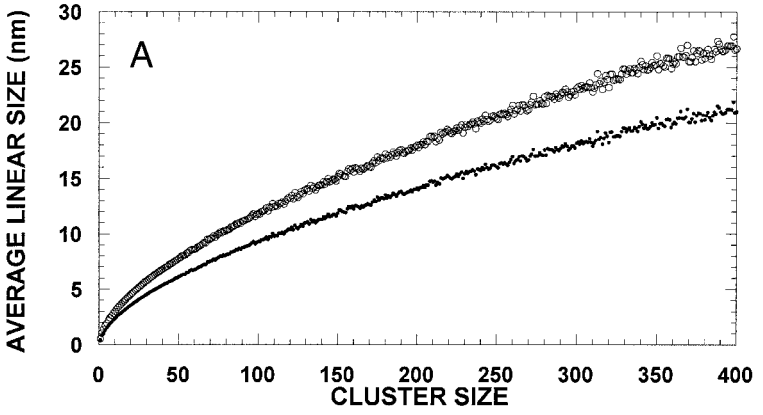

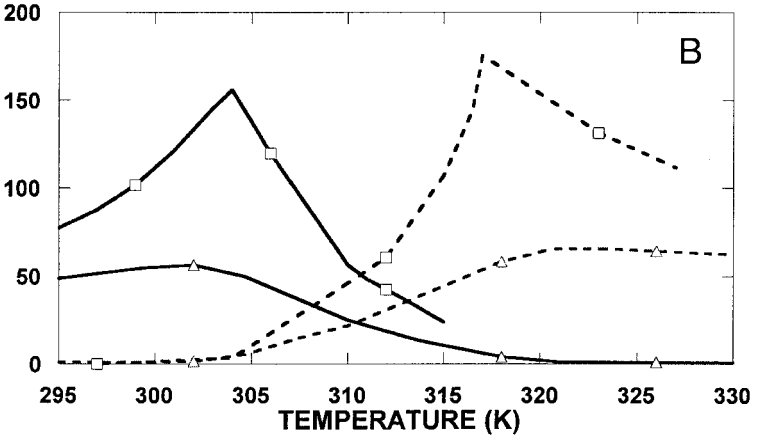

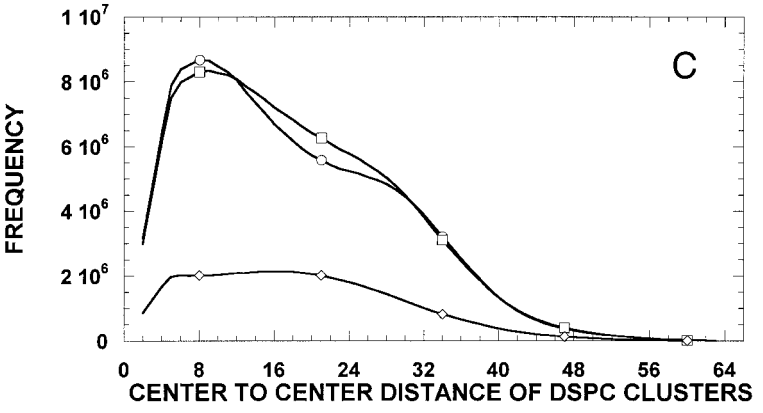

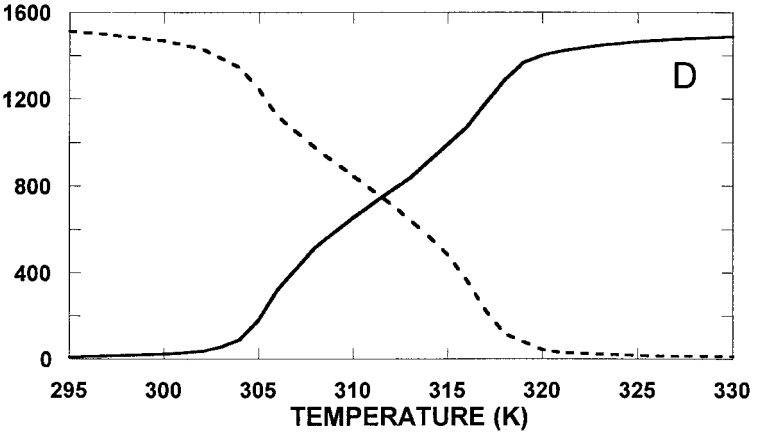

FIGURE 4 Calculated size, number, and center-to-center distance of clusters in equimolar DMPC/DSPC mixtures. (*A*) Calculated average linear size ⟨*ls*⟩ of gel (*closed circles*) and fluid clusters (*open circles*) at 305.3 K is plotted against the cluster size *S*. The linear cluster size is defined by Eq. 2. (*B*) Calculated temperature dependence of the average total size and average number of all the clusters except the largest one in each snapshot. *Open squares*: average total size; *open triangles*: average number of the clusters. Solid and dashed lines refer to fluid and gel clusters, respectively. (*C*) Calculated center-to-center distributions of DSPC clusters in equimolar DMPC/DSPC mixtures at 314 K (*squares*), 311 K (*circles*), and 283 K (*diamonds*). In each simulation 6000 equilibration cycles were followed by 1.2 million Monte Carlo cycles. The center-to-center distance is measured in lattice units. (*D*) Calculated temperature dependence of the average size of the largest cluster of the lattice. *Solid line*: fluid cluster; *dashed line*: gel cluster.

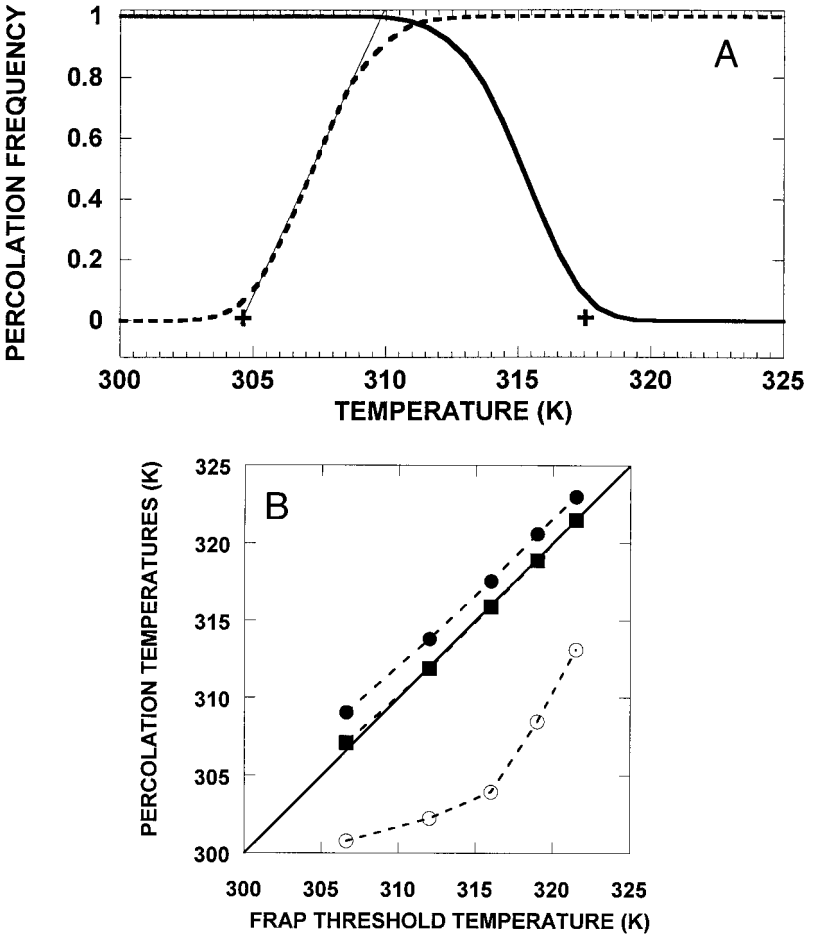

FIGURE 5 Percolation frequency curves and percolation threshold temperatures. (*A*) Calculated percolation frequency curves of gel and fluid clusters of equimolar DMPC/DSPC bilayers. *Dashed line*: fluid clusters; *solid line*: gel cluster. A straight line is fitted to the inflection point of the percolation frequency curve of fluid clusters and its intercept with the zero frequency line defines the percolation threshold temperature of fluid clusters (see cross at 304.6 K). The percolation threshold temperature of gel clusters is marked by a cross at 317.5 K. (*B*) Calculated percolation threshold temperatures versus FRAP threshold temperatures measured at different DMPC/DSPC mole fractions. *Closed circles*: percolation threshold temperatures of gel clusters; *open circles*: percolation threshold temperatures of fluid clusters; *closed squares*: temperatures at 0.36 percolation frequency of gel clusters.

by the small clusters. The ratio of the two curves in Fig. 4 *B* gives the average size of the small clusters. The maximum of the average size of small gel and fluid clusters is ~3 at 317 and 304 K, respectively.

Shankaram et al. (1992) determined the average size of fluid and gel domains in DMPC/DSPC bilayers by analyzing the ESR spectral lineshapes of spin-labeled DMPC. According to their analysis 1) the population of the gel (or fluid) state molecules increases by growth of domains, either from preexisting nuclei or from nuclei that are formed close to the onset temperature of the fluid-to-gel (or gel-to-fluid) transition; and 2) domains do not coalesce until the system approaches close to the point of percolation threshold temperature. In agreement with these qualitative conclusions of the ESR measurements our simulations show (see Fig. 4 *B*) that, e.g., the number of fluid clusters is practically constant from 299.2 K, the onset temperature of the gel-to-fluid transition (see Fig. 2), to ~303 K, where the domains start to coalesce. [We note that there is no significant change in the number of fluid clusters at the onset temperature of the transition. The number of fluid clusters slowly increases from a much lower temperature than the calorimetric onset temperature (see Fig. 7 in Sugar et al., 1999).] The calculated percolation threshold temperature of fluid clusters, 304.6 K, (see Fig. 5) is close to this temperature. Despite this qualitative agreement there are large differences in the values of the average cluster sizes. According to Sankaram et al. (1992), for example, the average size of fluid domains increases linearly from 1 to 1200 with increasing fraction of the fluid state molecules, while in our simulation the average size of the small fluid domains changes from 1 to 3. [Cluster size is defined by the number of hydrocarbon chains forming the cluster.] It is possible that in the ESR experiments the average cluster size is really larger than in the DMPC/DSPC mixture (with no spin-labeled lipid in it) because of the perturbing effect of the 3 mol % spin-labeled DMPC (personal communication with Dr. Shankaram). The other possibility is that in the spin-labeled system the domains are small, but incorrect assumptions biased the result of the analysis toward large cluster sizes. Actually, in the analysis of the ESR data it is assumed that at a given temperature and DMPC/DSPC mole fraction the size of each unconnected cluster is the same, and large enough to contain on average >10 spin-labeled lipid molecules. In these constant size clusters the more labeled lipid is in the cluster the broader the respective ESR spectrum.

TABLE 1 Experimental and calculated most frequent center-to-center distances of DSPC clusters in equimolar DMPC/DSPC mixtures

Temperature (K)	Average Coherence Length (Exp.) (nm)	Most Frequent Center-to-Center Distance (Calc.) (nm)	State
283	7.4 ± 0.5	7.7 (−2.6, +1.9)	gel
311	6.0 ± 0.5	5.2 (−0.61, +0.49)	gel/fluid mixed
314	6.3 ± 0.5	5.4 (−0.67, +0.67)	gel/fluid mixed

Experimental data were taken from Table 1 of Gliss et al. (1998). The average coherence length (interpreted by us as the most frequent center-to-center distance between DSPC domains) is the correlation length at the maximum of the integrated Bragg scattering intensity. The calculated values were obtained from the center-to-center distribution curves in Fig. 4 *C*, i.e., the most frequent center-to-center distance was multiplied by l_l at 311 and 314 K, and by l_g at 283 K. The error of the calculated data was estimated on the basis of the residual mean-square deviation between the simulated and the smoothed distribution by using a window size of 5.

Our simulation, however, resulted in a broad, asymmetric cluster size distribution that strongly peaks at cluster size $S = 1$. If these small clusters contain 0 or 1 spin label, then there is no line-broadening. If the small clusters contain 2 labels, then the smaller the cluster the larger the label concentration within the cluster and the respective line-broadening.

There is a rapidly growing number of direct observations of gel and fluid clusters in DMPC/DSPC mixtures (Gliss et al., 1998; Bagatolli and Gratton, 2000; Nielsen et al., 2000; Leidy et al., 2001a,b; Muresan and Lee, 2001). There are, however, vast differences between the observed cluster sizes and shapes depending on the type of the measurement, the construction, and thermal history of the sample. Atomic force microscopy (AFM) measurements on one layer of supported bilayer revealed gel cluster sizes from 10 to 50 nm (Gliss et al., 1998; Muresan and Lee, 2001), to several micrometers (Muresan and Lee, 2001; Leidy et al., 2001a) with irregular to rather circular cluster shapes. It was shown that the lateral diffusion of lipid molecules is five times smaller in supported bilayers (Sonnleitner et al., 1999) than in unsupported bilayers. Thus the clusters observed in different AFM measurements may belong to different nonequilibrium lateral distributions of the lipid molecules. Leidy et al. (2001b) tried to deposit two layers of bilayer to mica to accelerate equilibration. In this case they mainly observed clusters with straight edges, and assumed that the nuclei of these clusters were the remnants of the rippled phase. In this experiment, however, the utilized deposition technique may not guarantee the formation of only two layers of bilayer (comment after Dr. Leidy's presentation). Besides the problem of the equilibration it is also important to mention that very small (<10 nm) gel clusters in fluid matrix are not visible by AFM measurements (personal communication with Drs. Kay Yee Lee and Adrian Muresan).

The problems of low resolution and slow equilibration in measuring small clusters were resolved by Gliss et al. (1998). Grazing incidence diffraction of neutrons was utilized to measure the center-to-center distance between the perdeuterated DSPC clusters. The sample was several thousand multilayers of highly oriented, fully hydrated DMPC/DSPC bilayers. The average coherence lengths between the DSPC domains interpreted as the most frequent center-to-center distance of DSPC clusters and measured by Gliss et al. (1998) at three different temperatures are listed in Table 1. To make a comparison with these observed values the distribution of the center-to-center distance between the DSPC clusters was simulated by our model at the respective temperatures (see Fig. 4 *C*). [Cluster fragments located at the edges of the lattice were excluded from the distribution. The distribution has a shoulder at higher center-to-center distances only when the size distribution of the DSPC clusters is bimodal.] The calculated most frequent center-to-center distances, listed in the third column of Table 1, are within the error range of the measured average coherence length values. It is important to note that the calculated average linear size of the small DSPC clusters, ~1–1.5 nm, is considerably smaller than the calculated most frequent center-to-center distance, and thus the average coherence length measured by Gliss et al. (1998) is a rough upper estimate of the average linear size of the DSPC clusters.

The large cluster

In Fig. 4 *D* the average sizes of the largest gel and fluid clusters of each snapshot are plotted against the temperature. With decreasing temperature the average size of the largest gel cluster increases and eventually becomes comparable with the lattice size itself. Thus one can visualize this large cluster if the size of the bilayer is within the resolution of the microscope. Recently, Bagatolli and Gratton (2000) studied equimolar mixtures of DMPC/DSPC on giant unilamellar vesicles (of 30 μm diameter) by using fluorescence microscopy. From 321.2 K one or a small number of gel clusters of sizes comparable with the surface area of the giant vesicle were visible, and the size of these clusters increased with decreasing temperature. The above temperature, 321.2 K, is between the calculated percolation threshold of gel clusters (see Fig. 5 *A*) and the completion temperature of the gel-to-fluid transition (see Fig. 2). We think that the large cluster visualized by fluorescence microscopy is equivalent with the large cluster appearing in

the calculated, bimodal distribution of the cluster size (see above), and more than one large cluster can be observed if the lateral distribution of the lipid molecules in the giant vesicle did not attain the equilibrium (Michonova-Alexova and Sugar, 2001). According to our experience one can accelerate the attainment of the equilibrium distribution by means of freezing and thawing cycles (Liu et al., 1997).

Cluster percolation

A snapshot is percolated if a cluster, probably the largest one, spans the lattice either horizontally or vertically. The ratio of the number of percolated snapshots to the number of all the analyzed snapshots is the *percolation frequency*. In Fig. 5 *A* the temperature dependence of the percolation frequency is shown for both gel and fluid clusters in an equimolar mixture of DMPC/DSPC. A percolation threshold temperature can be calculated from the percolation frequency curve. For example, in the case of fluid clusters of an equimolar mixture of DMPC/DSPC the percolation threshold temperature is 304.6 K (see Fig. 5 *A*). At this temperature a shoulder appears in the cluster size distribution (see Fig. 3 *B*).

Vaz et al. (1989) were the first to measure FRAP threshold temperatures at different mole fractions of DMPC/DSPC bilayers and suggested identifying them with the percolation threshold temperatures of gel state clusters. In Fig. 5 *B* the percolation threshold temperatures calculated for gel phase clusters (*closed circles*) are plotted against the threshold temperatures obtained from FRAP experiments at different mole fractions. There is a strong correlation, with a constant difference of +1.8°C, between the calculated and measured threshold temperatures. There is complete agreement, however, if we plot the temperatures where the percolation frequency of the gel clusters is 0.36 (*closed squares*) against the FRAP threshold temperature. Thus the slight, but consistent, deviation between the calculated percolation threshold and measured FRAP threshold exists probably because rarely percolated gel clusters (at percolation frequencies from 0 to 0.36) cannot efficiently block the long-range diffusion of fluorescent probe molecules. It is important to note that there is no strong correlation between the calculated percolation threshold temperature of fluid clusters (*open circles*) and the measured FRAP threshold temperature (see Fig. 5 *B*). In the subsequent sections distinction is not made between the largest cluster and the smaller ones, i.e., every statistical analysis is performed on all the clusters in each snapshot.

Cluster perimeter and fractal dimension

In Fig. 6 *A* the average outer perimeter of fluid clusters $\langle PO \rangle$, is plotted against the cluster size *S*. The average outer perimeter increases with increasing cluster size. However, at cluster sizes comparable with the lattice size the average perimeter starts to decrease, and from this point one cannot differentiate outer from inner periphery. As an extreme example, the perimeter of a cluster of size *N* (the lattice size) is zero. This decline of the perimeter of large clusters is the consequence of the periodic boundary conditions. At a given cluster size the average outer perimeter of the fluid clusters slightly increases with decreasing temperature (data not shown); i.e., the periphery of fluid clusters is getting more rugged with decreasing temperature. The ruggedness of the perimeter can be characterized by the *effective fractal dimension* of the clusters, F_{eff}. One can get F_{eff} by fitting the following function to the average perimeter curve, $\langle PO(S) \rangle$ (Stauffer and Aharony, 1992):

$$\langle PO(S) \rangle = A \times S^{1/F_{\text{eff}}} \tag{6}$$

where A and F_{eff} are model parameters. Examples for different clusters and respective fractal dimensions are shown in the Appendix. By means of nonlinear curve-fitting the values of the model parameters of Eq. 6 have been determined, and the temperature dependence of the effective fractal dimension of gel and fluid clusters of equimolar DMPC/DSPC mixtures is plotted in Fig. 6 *B*. [When the size of the largest cluster of the snapshot is comparable with the lattice size, the curve-fitting either cannot be carried out or it is carried out only for the ascending section of the $\langle PO(S) \rangle$ curve.] The effective fractal dimension of fluid clusters increases with increasing temperature, while that of the gel clusters shows an opposite trend. One can calculate the lower limit of F_{eff} without simulations. At the onset of the transition only small clusters of size 0, 1, or 2 are present with respective perimeters of 0, 6, and 10. After fitting Eq. 6 to these 3 points one can get $F_{\text{eff}} = 1.357$. This lower limit is approached for gel clusters at 319.5 K and for fluid clusters at 302 K (see Fig. 6 *B*).

Similarly to the analysis of the snapshots one can analyze many AFM scans taken at the same temperature and DMPC/DSPC mole fraction, and determine the experimental value of the effective fractal dimension. A single AFM scan of supported equimolar DMPC/DSPC bilayers taken at 313 K was kindly provided to us by Drs. Ka Yee Lee and Adrian Muresan (University of Chicago). Because of the small number of clusters available for analysis in a single scan a broad range of the effective fractal dimension was obtained, 1.6 ± 0.1, while the effective fractal dimension calculated from the snapshots (simulated at 313 K) is 1.7 ± 0.03. [The clusters observed by AFM are much larger than the clusters in the snapshots. However, because of the self-similarity of fractal-like clusters, the fractal dimension should be independent from the cluster size.] Another type of fractal dimension, the so-called *capacity dimension* (Liebovitch, 1998) can be determined with less uncertainty for a single AFM scan. The capacity dimension characterizes the space-filling properties of the clusters. To evaluate the capacity of the clusters we cover the membrane surface

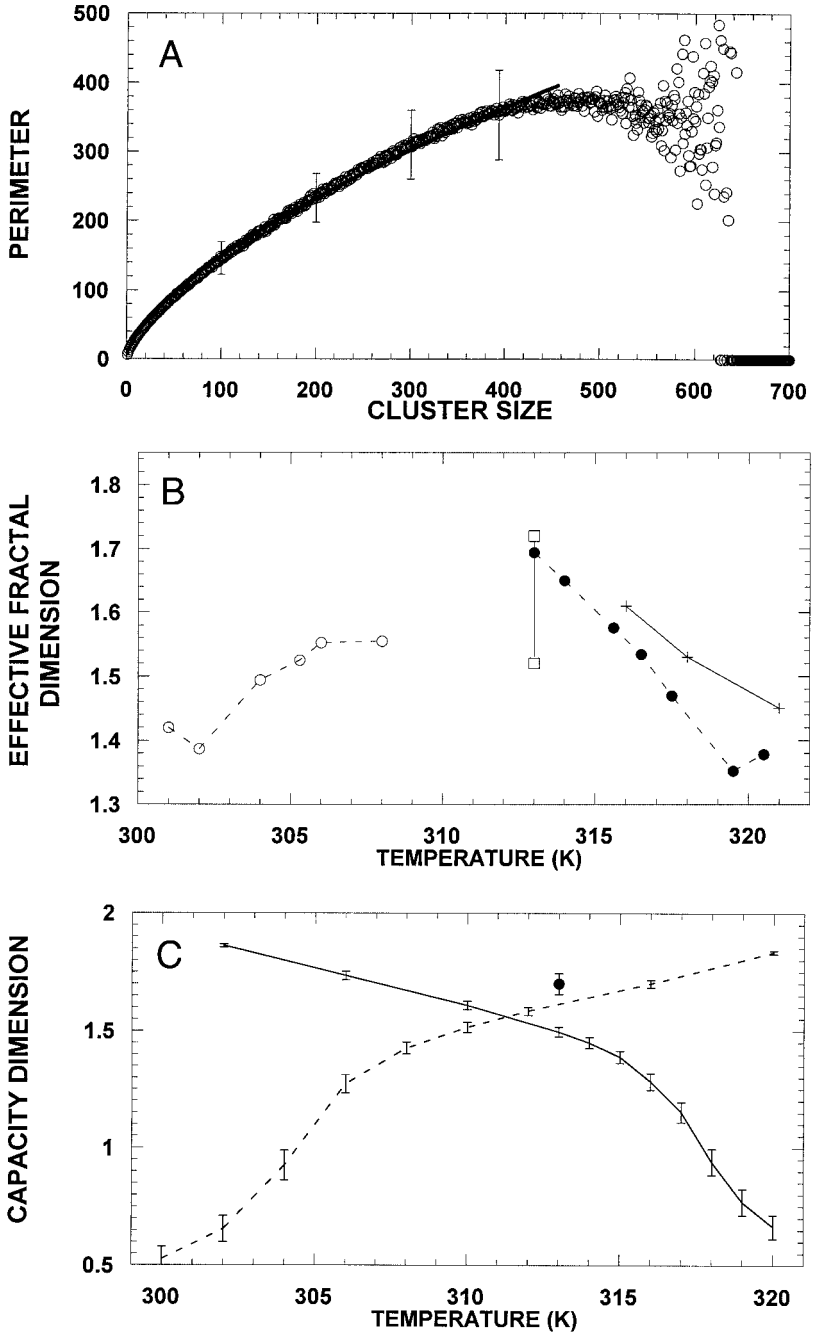

FIGURE 6 Clusters' outer perimeter and fractal dimensions. (*A*) Calculated average outer perimeter of fluid clusters of equimolar DMPC/DSPC bilayers. The average outer perimeter is plotted against the cluster size, *S*. Temperature: 306 K; *open circles*: simulated data; *solid line*: Eq. 6 is fitted to the ascending section of the simulated data. Estimated model parameters: $F_{\text{eff}} = 1.552 \pm 0.007$, $A = 7.68 \pm 0.12$. Error bars show the calculated standard deviations of the outer perimeter at certain cluster sizes. (*B*) Calculated effective fractal dimensions of fluid (*open circles*) and gel clusters (*closed circles*) of equimolar DMPC/DSPC bilayers are plotted against the temperature. Crosses and the connecting solid line mark the result of the obstacle aggregation model of Schram et al. (1996). Open squares connected by a solid line mark the upper and lower limit of the effective fractal dimension of gel clusters of an AFM scan (not shown). The scan, provided by Drs. Ka Yee Lee and Adrian Muresan (University of Chicago), was taken from a supported, equimolar DMPC/DSPC bilayer at 313 K, while the sample was in a solution of 8 mM $MgCl_2$. (*C*) Calculated capacity dimensions of fluid (*dashed line*) and gel clusters (*solid line*) of equimolar DMPC/DSPC bilayers are plotted against the temperature. The closed circle marks the capacity dimension of gel clusters obtained from the analysis of the same AFM scan mentioned in the legend to *B*. Error bars show the calculated standard deviations.

by squares of side length r. We find the smallest number of squares $M(r)$ needed to cover all the parts of the clusters. We then shrink the side length of the squares and again count the smallest number needed to cover the clusters. The capacity dimension is defined by the following limit:

$$F_{\text{cap}} = \lim_{r\to} \frac{d[\log M(r)]}{d\log(1/r)] } \tag{7}$$

Calculating the capacity dimension, a plot of $\log(M(r))$ versus $\log(1/r)$ was created for every snapshot (each containing 40×40 lattice points) and also for a single AFM scan (containing 480×480 pixels). The plots derived from the snapshots show a broken straight line. At large box sizes the slope is 2, while at smaller box sizes the slope of the straight line is smaller. The average of these smaller slopes was taken as the capacity dimension. In Fig. 6 *C* the capacity dimensions calculated for gel and fluid clusters are plotted against the temperature. The capacity dimension of the gel clusters in the AFM image and in the simulated snapshots at 313 K is 1.70 ± 0.04 and 1.49 ± 0.02,

respectively. The fractal dimensions calculated above are in rather good agreement with the observed fractal dimensions of the gel clusters despite the fact that the geometrical properties of the clusters of the supported bilayer could be perturbed by the bilayer-mica interaction and because the system may not have attained equilibrium. The comparison of Fig. 6 *B* and *C* shows that as a consequence of the different definitions, F_{eff} is different from F_{cap}. The difference is especially large at the onset of the transition when the size and number of the clusters is very small and the fractal dimensions are $F_{\text{eff}} \approx 1.357$ and $F_{\text{cap}} \approx 0$. It is, however, a common feature of these fractal dimensions that in the case of gel clusters they decrease with increasing temperature, while the trend is opposite for fluid clusters.

To clarify the impact of the fractality of small gel clusters on the diffusion coefficient measured by FRAP, Schram et al. (1996) have developed computer simulations of fluorescence recovery curves in a matrix obstructed with aggregates of point obstacles. Simulations have been performed to calculate the effective fractal dimension of the aggregate obstacles at different obstacle area fractions and aggregation probabilities. The results of these simulations can be compared with our results presented in Fig. 6 *B* if 1) the fractal dimension of the aggregate obstacles refers to the effective fractal dimension of the gel clusters; 2) the obstacle area fraction refers to the fraction of gel state lattice points; and 3) the obstacle area fractions in Shram's data are replaced by the respective temperatures. [These temperatures can be obtained from the melting curve of the equimolar mixture of DMPC/DSPC (see, e.g., Fig. 3 *B* in Sugar and Biltonen, 2000).] In Fig. 6 *B* the solid line marked by crosses has been derived from Schram's data (see Table 1, at $P_{\text{agg}} = 1$ in Schram et al., 1996) and it is close to the data points obtained from our simulations for the effective fractal dimension of the gel clusters at different temperatures. It is important to note that Schram's data at $P_{\text{agg}} = 1$ were utilized because at this aggregation probability the percolation frequencies of the aggregate obstacles are closest to the percolation frequencies of the gel clusters in our DMPC/DSPC model. [The percolation frequency of the obstacle aggregates (at $P_{\text{agg}} = 1$) changes from 0 to 1 when the obstacle area fraction changes from 0.3 to 0.4, while in our simulations the same change of the percolation frequency of the gel clusters takes place when the fraction of the gel state lattice points changes from 0.24 to 0.5 (see Fig. 8 *C* in Sugar et al., 1999).]

So far it has been shown that not only the calculated excess heat capacity curves, but also calculated geometrical properties of the clusters, such as percolation thresholds, fractal dimensions, and center-to-center distances, are in quantitative agreement with the experimental data. In the rest of the paper, by using the same model (with the same model parameter values), other geometrical properties of the clusters will be calculated. Currently, experimental data are not available to confirm the validity of these calculated results. However, the success of our model in correctly calculating other geometrical properties increases the possibility that these theoretical results are correct, too.

Inner islands of clusters

In Fig. 7 *A* the average number of inner islands $\langle NI \rangle$ are plotted against the size of the host fluid cluster, *S*. Up to $S = 6$ the average number of inner islands is exactly zero, and then it gradually increases.

In Fig. 7 *B* the average size of the inner islands, $\langle SI \rangle$, is plotted against the size of the host fluid cluster, *S*. There is no inner island at $S < 6$. From $S = 6$ the average size of the inner islands gradually increases from 1 to ~2.

The data in Fig. 7 are taken at three different temperatures: 302, 305.3, and 306 K. With increasing temperature the upper bound of the size of the host fluid clusters increases from 200 to ~600; however, at a given size of the host cluster $\langle NI \rangle$ and $\langle SI \rangle$ do not show any significant temperature dependence. The average number of inner island versus the size of the host cluster can be described by the following power function (see *solid line* in Fig. 7 *A*):

$$\langle NI \rangle = D_1 \times S^{D_2}. \tag{8}$$

However, the average size of an inner island versus the size of the host cluster can be described by the following exponential function (see *solid line* in Fig. 7 *B*):

$$\langle SI \rangle = 1 + E_1 \times (1 - e^{-E_2 \times S}). \tag{9}$$

The model parameters of Eqs. 8 and 9 have been obtained by means of nonlinear parameter estimation (see the legend to Fig. 7). It is important to note that similar results were obtained for the average number and size of inner islands in host gel clusters.

Inner islands are visible on AFM scans of equimolar DMPC/DSPC bilayers when their size is larger than the resolution of AFM (>10 nm). Direct comparison, however, cannot be made with the calculated results when the size of most of the inner islands is below this resolution.

Cluster arms

One may expect that the number of arms linearly increases with the outer perimeter of the cluster. In Fig. 8 *A* the average number of arms of the fluid clusters $\langle NA(S) \rangle$ is plotted against the clusters' average outer perimeter $\langle PO(S) \rangle$. Except for clusters of $S \leq 8$ the simulated data support the above expected linearity (data are not shown for gel clusters), i.e.,

$$\langle NA(S) \rangle = (1/B) \times \langle PO(S) \rangle + C \tag{10}$$

The estimated values of the model parameters, $B \approx 30$ and $C \approx 1.25$, do not show significant temperature or state dependence. Thus the average perimeter per arm is ~30, or

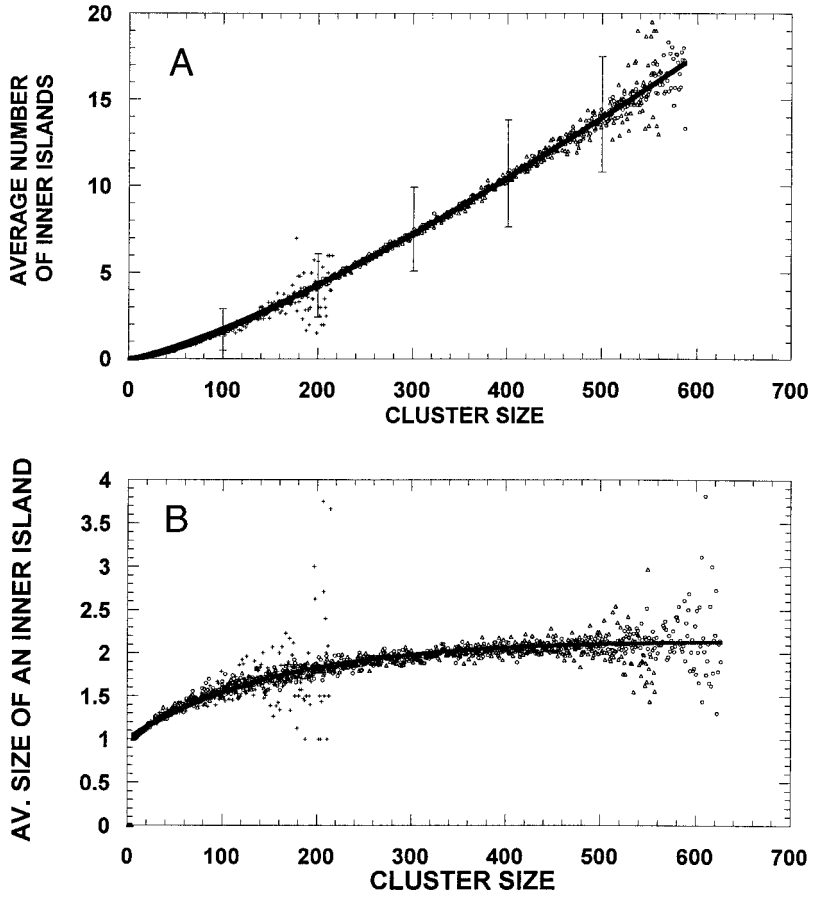

FIGURE 7 Calculated average number and average size of inner islands in the fluid clusters of equimolar DMPC/DSPC bilayers. (*A*) Average number of inner islands versus size of the host fluid cluster. Equation 8 is fitted to the simulated data (*solid line*). Estimated parameters are $D_1 = 0.00427 \pm 0.00009$ and $D_2 = 1.304 \pm 0.0034$. The correlation coefficient is $r = 0.9994$. Error bars show the calculated standard deviations. (*B*) Average size of inner islands versus size of the host fluid cluster. Equation 9 is fitted to the simulated data (*solid line*). Estimated parameters are $E_1 = 1.09 \pm 0.01$ and $E_2 = 0.0072 \pm 0.0002$. The correlation coefficient is $r = 0.977$. Cross: 302 K; *open triangles*: 305.3 K; *open circles*: 306 K.

in nanometers it is $15 \times [(l_g + l_l)/2] \approx 8.2$ nm (see Eq. 3), where $(l_g + l_l)/2$ is the estimated interchain distance at the gel-fluid interface.

By substituting Eq. 6 into Eq. 10 one can get the following relationship between the cluster size S and the number of arms:

$$\langle NA(S)\rangle = (A/B) \times S^{1/F_{eff}} + C \qquad (11)$$

Fig. 8 *B* demonstrates the excellent agreement between the simulated $\langle NA(S)\rangle$ data and the curve calculated from Eq. 11.

Association of clusters

Cluster growth and decrease is the result of intracluster state change or intercluster diffusion, i.e., association and dissociation of clusters. By using Eqs. 6, 8, and 9, derived for the average outer perimeter, number, and size of inner islands of the clusters, one can calculate the change of the outer and inner perimeters during the association process. When two clusters of size S_1 and S_2 associate, the average change of the outer perimeter is

$$\Delta PO = \langle PO(S_1 + S_2)\rangle - [\langle PO(S_1)\rangle + \langle PO(S_2)\rangle]$$
$$= A[(S_1 + S_2)^{1/F_{eff}} - S_1^{1/F_{eff}} - S_2^{1/F_{eff}}] \qquad (12)$$

It can be shown that ΔPO is negative for any sizes of the associating clusters. This is the case because molecules situated at the contact points of the associating clusters become internal molecules of the associated cluster. The change of the inner perimeter during the association is

$$\Delta PI = \langle (PI(S_1 + S_2)\rangle - [\langle PI(S_1)\rangle + \langle PI(S_2)\rangle] \qquad (13)$$

where $\langle PI(S)\rangle$ is the total average perimeter of the inner islands in a host cluster of size S. If, similarly to Eq. 6, the average perimeter of an inner island of size SI is $A_i \times (SI)^{1/F_i}$, then the total average perimeter of the inner islands is

$$\langle PI(S)\rangle = \langle NI(S)\rangle \times A_i \times \langle SI(S)\rangle^{1/F_i} \qquad (14)$$

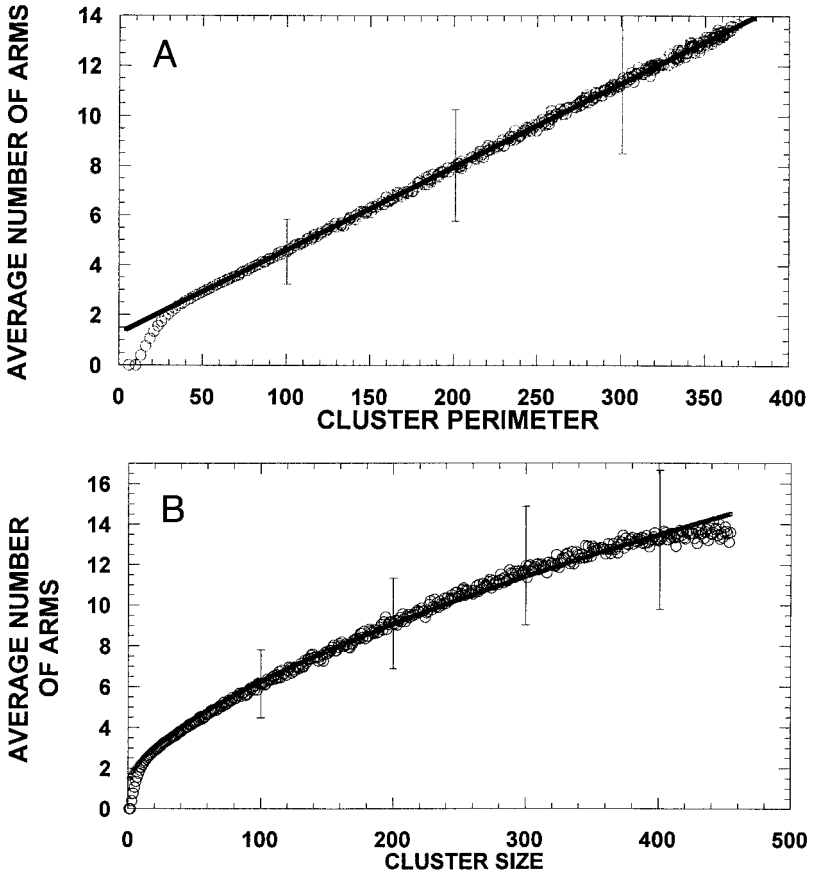

FIGURE 8 Calculated average number of arms of fluid clusters of equimolar DMPC/DSPC bilayers. Temperature: 306 K; *open circles*: simulated data. Error bars show the calculated standard deviations. (*A*) Average number of arms versus cluster's average outer perimeter. *Solid line*: Eq. 10 is fitted to the straight section of the simulated curve. Estimated model parameters: $B = 29.82 \pm 0.05$, $C = 1.25 \pm 0.01$. (*B*) Average number of arms versus cluster size. The solid line is calculated from Eq. 11 by using the above values for B and C, while the values for A and F_{eff} are given in the legend to Fig. 6 *A*.

where $\langle NI(S)\rangle$ and $\langle SI(S)\rangle$ can be calculated from Eqs. 8 and 9, respectively. Calculating the change of the inner perimeter one may assume that the effective fractal dimension, F_i, and fractal factor, A_i, of the inner islands are equal with the fractal parameters of the host clusters themselves, e.g., $A = A_i = 7.7$ and $F_{\text{eff}} = F_i = 1.552$ (see legend to Fig. 6 *A*). It can be shown that ΔPI is positive for any sizes of the associating clusters. This is the case because molecules internalized during the association process may form the edge of inner islands in the associated cluster. The sum of these two changes $\Delta PO + \Delta PI$ gives the change of the total perimeter during the association process. The calculations show that the total perimeter always decreases during the association process, i.e., the increase of the inner perimeter cannot compensate for the decrease of the outer perimeter. This is the case because during the association process there are always truly internalized molecules that are not situated at the interface of inner islands. Finally, the analysis of Eqs. 12 and 13 shows that the largest changes of PO, PI, and $PO + PI$ take place when equal-size clusters associate.

CONCLUSIONS

A simple two-state, two-component Ising-type model describes the gel-fluid transition of DMPC/DSPC bilayers as a continuous transition through equilibrium states. The calculated excess heat capacities, percolation threshold temperatures of gel clusters, most frequent center-to-center distances of DSPC clusters, and fractal dimensions of gel clusters are in quantitative agreement with the respective DSC, FRAP, neutron diffraction, and AFM data. The simulations demonstrate that nanoscale gel domains, detected by neutron diffraction, can coexist with one large gel cluster of size comparable with the membrane surface area detected by fluorescence microscopy. Equations—derived for the average outer perimeter, average number and average size of internal islands of clusters—are utilized to investigate the process of cluster association.

APPENDIX

Let us consider three examples of clusters and respective fractal parameters.

First, in the case of circular clusters, where the periphery is smooth, the following relationship holds for the periphery:

$$po = 2\sqrt{\pi} \times s^{1/2} \tag{15}$$

where s is the surface area of the cluster. The dimensionless form of Eq. 15 can be obtained by substituting Eqs. 1 and 3 into Eq. 15:

$$PO = 4\sqrt{\pi\sqrt{3}/2} \times S^{1/2} \tag{16}$$

and by comparing Eq. 16 with Eq. 6 factor A is $A = 6.6$ and the effective fractal dimension is $F_{\text{eff}} = 2$.

Second, in the case of ramified clusters, such as treelike clusters with long branches of similar thickness, w, the perimeter is related to the cluster's surface area, s, as follows: $po \approx (2/w) \times s$. After substituting Eqs. 1 and 3 we get the following dimensionless form of the above relationship: $PO \approx (4\sqrt{3}/W) \times S$. [The relationship between w and W, the thickness in unit length, is defined by $w = (W/2) \times l$, an equation similar to Eq. 3.] By comparing this equation with Eq. 6 the effective fractal dimension of the treelike clusters is $F_{\text{eff}} = 1$ and the fractal factor is $A = 4\sqrt{3}/W$.

Finally, let us consider ringlike clusters with similar ring thickness, w, and with ring diameters $d \gg w$. In this case the outer perimeter, po, is related to the cluster's surface area, s, as follows: $po \approx (1/w) \times s$. By means of Eqs. 1 and 3 the dimensionless form of this relationship is $PO \approx (2\sqrt{3}/W) \times S$, and thus the effective fractal dimension of the ringlike clusters is $F_{\text{eff}} = 1$ and the fractal factor is $A = 2\sqrt{3}/W$.

The first and last examples show that one can get different fractal dimensions for clusters with similar outer periphery, but with different inner structure of the clusters. One can define fractal dimension, which is characteristic to the shape of the outer periphery of the clusters and not to the clusters' inner structure, by using the following corrected form of Eq. 6:

$$\langle PO(S) \rangle = A_{\text{corr}} \times L(S)^{1/F_{\text{corr}}} \tag{17}$$

where $L(S)$ is the number of lattice points surrounded by the outer periphery of a cluster of size S. Because L is independent from the inner structure of the clusters the effective fractal dimension, F_{corr}, and the fractal factor, A_{corr}, are solely characteristic of the ruggedness of the outer periphery of the clusters. In the case of our DMPC/DSPC model the number of lattice points belonging to the inner islands of the host cluster can be estimated by $\langle NI(S) \rangle \times \langle SI(S) \rangle$ and thus $L(S) \approx S + \langle NI(S) \rangle \times \langle SI(S) \rangle$. After substituting Eqs. 8 and 9 into this relationship one can realize that $L(S) \approx S$, and thus the corrected form of Eq. 6 will not result in significantly different fractal parameter values.

The authors thank Drs. Ka Yee Lee and Adrian Muresan for the valuable discussions on atomic force microscopy and for providing us an AFM scan, and Kevin Kelliher for processing the AFM image file. We thank Drs. Thomas E. Thompson, Rodney L. Biltonen, Mantripragada B. Sankaram, Thomas Heimburg, and Vincent Schram for their thorough and insightful comments. Dr. Sugar acknowledges Mrs. Lawrence Garner's generous support.

This work was supported by Pfizer Inc., and by American Heart Association Grant 9950320N.

REFERENCES

Almeida, P. F. F., W. L. C. Vaz, and T. E. Thompson. 1992. Lateral diffusion and percolation in two-phase-two-component lipid bilayers: topology of the solid-phase domains in-plane and across the lipid bilayer. *Biochemistry.* 31:7198–7210.

Almeida, P. F., A. K. Hinderliter, C. E. Creutz, and R. L. Biltonen. 2001. Domain formation in a fluid mixed lipid bilayer modulated through binding of the C2 protein motif. *Biophys. J.* 80:185*a*. (Abstr.).

Bagatolli, L. A., and E. Gratton. 2000. A correlation between lipid domain shape and binary phospholipid mixture composition in free standing bilayers: a two-photon fluorescence microscopy study. *Biophys. J.* 79: 434–447.

Bergelson, L. O., K. Gawrisch, J. A. Feretti, and R. Blumenthal, editors. 1995. Special issue on domain organization in biological membranes. *Mol. Membr. Biol.* 12:1–162.

Binder, K., and D. Stauffer. 1986. Monte Carlo studies of systems with disorder. *In* Monte Carlo Methods in Statistical Physics, Chapter 8. K. Binder, editor. Springer-Verlag, Berlin, Heidelberg, New York, Tokyo.

Binder, K., and D. Stauffer. 1987. Monte Carlo studies of "random" systems. *In* Applications of the Monte Carlo Method in Statistical Physics, Chapter 8. K. Binder, editor. Springer-Verlag, Berlin, Heidelberg, New York, Tokyo.

Brumbaugh, E. E., and C. Huang. 1992. Parameter estimation in binary mixtures of phospholipids. *Methods Enzymol.* 210:521–539.

Brumbaugh, E. E., M. L. Johnson, and C. Huang. 1990. Non-linear least squares analysis of phase diagrams for non-ideal binary mixtures of phospholipids. *Chem. Phys. Lipids.* 52:69–78.

Brumm, T., K. Jørgensen, O. G. Mouritsen, and T. M. Bayerl. 1996. The effect of increasing membrane curvature on the phase transition and mixing behavior of a dimiristoyl-*sn*-glycero-3-phosphatidylcholine/distearoyl-*sn*-glycero-3-phosphatidylcholine lipid mixture as studied by Fourier transform infrared spectroscopy and differential scanning calorimetry. *Biophys. J.* 70:1373–1379.

Caille, A., D. Pink, F. DeVerteuil, and M. J. Zuckermann. 1980. Theoretical models for quasi-two-dimensional mesomorphic monolayers and membrane bilayers. *Can. J. Physics.* 58:581–611.

Chiu, S.-W., M. Clark, V. Balaji, S. Subramanian, H. L. Scott, and E. Jacobsson. 1995. Incorporation of surface tension into molecular dynamics simulations of an interface: a fluid phase lipid bilayer membrane. *Biophys. J.* 69:1230–1245.

Coniglio, A. 1989. Fractal structure of Ising and Potts clusters: exact results. *Phys. Rev. Lett.* 62:3054–3057.

Damodoran, K. V., and K. M. Merz. 1994. A comparison of DMPC- and DLPE-based lipid bilayers. *Biophys. J.* 66:1076–1087.

Dolainsky, C., P. Karakatsanis, and T. M. Bayerl. 1997. Lipid domains as obstacles for lateral diffusion in supported bilayers probed at different time and length scales by two-dimensional exchange and field gradient solid state NMR. *Phys. Rev. E.* 55:4512–4521.

Doniach, S. 1978. Thermodynamic fluctuations in phospholipid bilayers. *J. Chem. Phys.* 68:4912–4916.

Edidin, M. 1990. Molecular associations and membrane domains. *Curr. Top. Membr. Transp.* 36:81–96.

Feller, S. E., Y. Zhang, and R. W. Pastor. 1995. Computer simulation of liquid/liquid interfaces. Surface tension-area dependence of bilayer and monolayer. *J. Chem. Phys.* 103:10267–10276.

Gliss, C., H. Clausen-Schaumann, R. Gunther, S. Odenbach, O. Randl, and T. M. Bayerl. 1998. Direct detection of domains in phospholipid bilayers by grazing incidence diffraction of neutrons and atomic force microscopy. *Biophys. J.* 74:2443–2450.

Hao, M.-H., and H. A. Scheraga. 1994. Monte Carlo simulation of a first-order transition for protein folding. *J. Phys. Chem.* 98:4940–4948.

Hao, M.-H., and H. A. Scheraga. 1996. Optimizing potential functions for protein folding. *J. Phys. Chem.* 100:14540–14548.

Heimburg, T., and R. L. Biltonen. 1996. A Monte Carlo simulation study of protein-induced heat capacity changes and lipid-induced protein clustering. *Biophys. J.* 70:84–96.

Heimburg, T., and D. Marsh. 1996. Thermodynamics of the interaction of proteins with lipid membranes. *In* Biological Membranes. A Molecular Perspective from Computation and Experiment. K. M. Merz and B. Roux, editors. Birkhauser, Boston. 405–462.

Huang, P., J. J. Perez, and G. H. Loew. 1994. Molecular dynamics simulations of phospholipid bilayers. *J. Biomol. Struct. Dyn.* 11: 927–956.

Ipsen, J. H., and O. G. Mouritsen. 1988. Modelling the phase equilibria in two-component membranes of phospholipids with different acyl-chain lengths. *Biochim. Biophys. Acta.* 944:121–134.

Ising, E. 1925. Beitrag zur Theorie des Ferromagnetismus. *Z. Phys.* 21: 253–258.

Jan, N., T. Lookman, and D. A. Pink. 1984. On computer simulation methods used to study models of two-component lipid bilayers. *Biochemistry.* 23:3227–3231.

Jerala, R., P. F. F. Almeida, and R. L. Biltonen. 1996. Simulation of the gel-fluid transition in a membrane composed of lipids with two connected acyl chains: application of a dimer-move step. *Biophys. J.* 71: 609–615.

Jørgensen, K., M. M. Sperotto, O. G. Mouritsen, J. H. Ipsen, and M. J. Zuckermann. 1993. Phase equilibria and local structure in binary lipid bilayers. *Biochim. Biophys. Acta.* 1152:135–145.

Klein, W., and A. Coniglio. 1981. Thermal phase transitions at the percolation threshold. *Phys. Lett. A.* 84:83–84.

Knoll, W., K. Ibel, and E. Sackmann. 1981. Small-angle neutron scattering study of lipid phase diagrams by the contrast variation method. *Biochemistry.* 20:6379–6383.

Leidy, C., W. F. Wolkers, K. Jørgensen, O. G. Mouritsen, and J. H. Crowe. 2001a. Lateral organization and domain formation in a two-component lipid membrane system. *Biophys. J.* 80:1819–1828.

Leidy, C., T. Kaasgaard, T. V. Ratto, M. Longo, O. G. Mouritsen, J. H. Crowe, and K. Jørgensen. 2001b. Lipid domain growth and shape changes as a function of temperature in binary lipid mixtures visualized by atomic force microscopy. *Biophys. J.* 80:332*a*. (Abstr.).

Liebovitch, L. S. 1998. Fractal and Chaos. Simplified for the Life Sciences. Oxford University Press, New York, Oxford. 50–51.

Liu, F., I. P. Sugar, and P. L.-G. Chong. 1997. Cholesterol and ergosterol superlattices in three-component liquid crystalline lipid bilayers as revealed by dehydroergosterol fluorescence. *Biophys. J.* 72:2243–2254.

Lu, D., I. Vavasour, and M. R. Morrow. 1995. Smoothed acyl chain orientational order parameter profiles in dimyristoylphosphatidylcholine-distearoylphosphatidylcholine mixtures: a ^{2}H-NMR study. *Biophys. J.* 68:574–583.

Mabrey, S., and J. M. Sturtevant. 1976. Investigation of phase transitions of lipids and lipid mixtures by high sensitivity differential scanning calorimetry. *Proc. Natl. Acad. Sci. U.S.A.* 73:3862–3866.

Marrink, S. J., and H. J. C. Berendsen. 1994. Simulation of water transport through a lipid membrane. *J. Phys. Chem.* 98:4155–4168.

Mendelsohn, R., G. L. Liang, H. L. Strauss, and R. G. Snyder. 1995. IR spectroscopic determination of gel state miscibility in long-chain phosphatidylcholine mixtures. *Biophys. J.* 69:1987–1998.

Mendelsohn, R., and J. Maisano. 1978. Use of deuterated phospholipids in Raman spectroscopic studies of membrane structure. I. Multilayers of dimyristoylphosphatidylcholine (and its $-d_{54}$ derivative) with distearoylphosphatidylcholine. *Biochim. Biophys. Acta.* 506:192–201.

Merz, K. 1997. Molecular dynamics simulations of lipid bilayers. *Curr. Opin. Struct. Biol.* 7:511–517.

Michonova-Alexova, E., and I. P. Sugar. 2001. Size distribution of gel and fluid clusters in DMPC/DSPC lipid bilayers. A. Monte Carlo simulation study. *J. Phys. Chem. B.* 105: in press.

Muresan, A. S., and K. Y. C. Lee. 2001a. Formation of nano-scale compartments in phospholipid membranes. *Biophys. J.* 80:540*a* (Abstr.). (This is a title modified by the authors after the abstract submission.)

Nagle, J. F. 1973. Theory of biomembrane phase transition. *J. Chem. Phys.* 58:252–264.

Nagle, J. F., and S. Tristram-Nagle. 2000. Structure of lipid bilayers. *Biochim. Biophys. Acta.* 1469:159–195.

Nielsen, L. K., A. Vishnyakov, K. Jørgensen, T. Bjornholm, and O. G. Mouritsen. 2000. Nanometre-scale structure of fluid lipid membranes. *J. Phys. Condens. Matter.* 12:A309–A314.

Orci, L., B. Thorens, M. Ravazzola, and H. F. Lodish. 1989. Localization of the pancreatic beta cell glucose transporter to specific plasma membrane domains. *Science* (*Wash. DC*). 245:295–297.

Pedersen, S., K. Jorgensen, T. E. Baekmark, and O. G. Mouritsen. 1996. Indirect evidence for lipid-domain formation in the transition region of phospholipid bilayers by two-probe fluorescence energy transfer. *Biophys. J.* 71:554–560.

Perera, L., U. Essmann, and M. L. Berkowitz. 1996. The origin of the hydration interaction of lipid bilayers from MD simulation of dipalmitoylphosphatidylcholine membranes in gel and liquid crystalline phases. *Langmuir.* 12:4519–4531.

Piknova, B., D. Marsh, and T. E. Thompson. 1996. Fluorescence-quenching study of percolation and compartmentalization in two-phase lipid bilayers. *Biophys. J.* 71:892–897.

Priest, R. 1980. Landau phenomenological theory of one and two component phospholipid bilayers. *Mol. Cryst. Liq. Cryst.* 60:167–184.

Risbo, J., M. Sperotto, and O. G. Mouritsen. 1995. Theory of phase equilibria and critical mixing points in binary lipid membranes. *J. Chem. Phys.* 103:3643–3656.

Rodgers, W., and M. Glaser. 1991. Characterization of lipid domains in erythrocyte membranes. *Proc. Natl. Acad. Sci. U.S.A.* 88:1364–1368.

Rothberg, K. G., Y. Ying, J. F. Kolhouse, B. A. Kamen, and R. G. W. Anderson. 1990. The glycosphingolipid-linked folate receptor internalizes folate without entering the clathrin-coated pitendocytic pathway. *J. Cell Biol.* 110:637–649.

Sankaram, M. B., D. Marsh, and T. E. Thompson. 1992. Determination of fluid and gel domain sizes in two-component, two-phase lipid bilayers: an electron spin resonance spin label study. *Biophys. J.* 63:340–349.

Sankaram, M. B., and T. E. Thompson. 1992. Deuterium magnetic resonance study of phase equilibria and membrane thickness in binary phospholipid mixed bilayers. *Biochemistry.* 31:8258–8268.

Schram, V., H.-N. Lin, and T. E. Thompson. 1996. Topology of gel phase domains and lipid mixing properties in phase-separated two-component phosphatidylcholine bilayers. *Biophys. J.* 71:1811–1822.

Scott, H. L. 1977. Monte Carlo studies of the hydrocarbon region of lipid bilayers. *Biochim. Biophys. Acta.* 469:264–271.

Scott, H. L., E. Jacobson, and S. Subramaniam. 1998. Simulation of lipid membranes with atomic resolution. *Comp. Phys.* 12:328–334.

Shakhnovich, E. I., and A. M. Gutin. 1993. Engineering of stable and fast-folding sequences of model proteins. *Proc. Natl. Acad. Sci. U.S.A.* 90:7195–7199.

Sonnleitner, A., G. J. Schutz, and Th. Schmidt. 1999. Free Brownian motion of individual lipid molecules in biomembranes. *Biophys. J.* 77:2638–2642.

Stauffer, D. 1985. Introduction to Percolation Theory. Taylor and Francis, London and Philadelphia. 110.

Stauffer, D., and A. Aharony. 1992. Introduction to Percolation Theory. Taylor and Francis, London, Washington, DC. 61.

Sugar, I. P., and R. L. Biltonen. 2000. Structure-function relationships in two-component phospholipid bilayers. A Monte Carlo simulation approach using a two-state model. *Methods Enzymol.* 323:340–372.

Sugar, I. P., R. L. Biltonen, and N. Mitchard. 1994. Monte Carlo simulation of membranes: phase transition of small unilamellar dipalmitoylphosphatidylcholine vesicles. *Methods Enzymol.* 240:569–593.

Sugar, I. P., and G. Monticelli. 1985. Interrelationships between the phase diagrams of the two-component phospholipid bilayers. *Biophys. J.* 48: 283–288.

Sugar, I. P., T. E. Thompson, and R. L. Biltonen. 1999. Monte Carlo simulation of two-component bilayers: DMPC/DSPC mixtures. *Biophys. J.* 76:2099–2110.

Sun, H., M. Mezei, R. Fye, and C. J. Benham. 1995. Monte Carlo analysis of conformational transitions in superhelical DNA. *J. Chem. Phys.* 103:8653–8665.

Sun, H., and I. P. Sugar. 1997. Acceleration of convergence to the thermodynamic equilibrium by introducing shuffling operations to the Metropolis algorithm of Monte Carlo simulations. *J. Phys. Chem. B.* 101: 3221–3227.

Suurkuusk, J., B. R. Lentz, Y. Barenholz, R. Biltonen, and T. E. Thompson. 1976. A calorimetric and fluorescent probe study of the gel-liquid crystalline phase transition in small, single-lamellar dipalmitoylphosphatidylcholine vesicles. *Biochemistry.* 15:1393–1401.

Thompson, T. E., M. B. Shankaram, R. L. Biltonen, D. Marsh, and W. L. C. Vaz. 1995. Effects of domain structure on in-plane reactions and interactions. *Mol. Membr. Biol.* 12:157–162.

Tocanne, J. F. 1992. Detection of lipid domains in biological membranes. *Comm. Mol. Cell. Biophys.* 8:53–72.

Tu, K., D. J. Tobias, and M. L. Klein. 1995. Constant pressure and temperature molecular dynamics simulation of fully hydrated liquid crystal phase dipalmitoylphosphatidylcholine bilayer. *Biophys. J.* 69: 2558–2562.

van Dijck, P. W. M., A. J. Kaper, H. A. J. Oonk, and J. De Gier. 1977. Miscibility properties of binary phosphatidylcholine mixtures. *Biochim. Biophys. Acta.* 470:58–69.

Vaz, W. L. C., E. C. C. Melo, and T. E. Thompson. 1989. Translational diffusion and fluid domain connectivity in two-component, two-phase phospholipid bilayers. *Biophys. J.* 56:869–876.

Von Dreele, P. H. 1978. Estimation of lateral species separation from phase transitions in nonideal two-dimensional lipid mixtures. *Biochemistry.* 17:3939–3943.

Wilkinson, D. A., and J. F. Nagle. 1979. Dilatometric study of binary mixtures of phosphatidylcholines. *Biochemistry.* 18:4244–4249.

Yue, K., and K. A. Dill. 1995. Forces of tertiary structural organization in globular proteins. *Proc. Natl. Acad. Sci. U.S.A.* 92:146–150.

Zhou, F., and K. Schulten. 1995. Molecular dynamics study of a membrane-water interface. *J. Phys. Chem.* 99:2194–2207.